Droop-controlled inverter-based microgrids are robust to clock drifts

Johannes Schiffer, Romeo Ortega, Christian A. Hans, Jörg Raisch

***Abstract*— Clock drift in digital controllers is of great relevance in many applications. Since almost all real clocks exhibit drifts, this applies in particular to networks composed of several individual units, each of which being operated with its individual clock. In the present work, we investigate the effect of clock drifts in inverter-based microgrids. Via a suitable model that incorporates this phenomenon, we prove that clock inaccuracies hamper synchronization in microgrids, in which the individual inverters are operated with a fixed uniform constant electrical frequency. In addition, we show that the well-known frequency droop control renders stability of a lossless microgrid robust with respect to clock inaccuracies. This claim is established by using stability results reported previously by the authors for lossless inverter-based microgrids with ideal clocks. We also discuss the effect of clock drifts on active power sharing. The analysis is illustrated via a simulation example.**

I. Introduction

As a consequence of political and environmental goals together with technological advances, the worldwide use of renewable energies has increased significantly in recent years. This development not only changes the mix of the generation structure, but also strongly affects the power system structure and its operation as a whole [1]. In particular, most renewable power plants are relatively small-sized in terms of their generation power. Therefore, they are often connected to the power system at the medium (MV) and low voltage (LV) levels. Such units are commonly denoted as distributed generation (DG) units and are mostly interfaced to the network via AC inverters. The latter are power electronic devices, which possess significantly different physical characteristics from synchronous generators (SGs). This implies that new control and operation strategies are needed in networks with a large share of DG units [2].

Microgrids are foreseen to be a promising solution to address these changes by enabling an efficient and reliable integration of large shares of renewable DG units in the electrical power system [1], [3], [4]. A microgrid is a locally controllable subset of a larger electrical network. It is composed of several DG units, storage devices and loads. One main feature of a microgrid is that it can be operated either in grid-connected or in islanded mode, i.e., in a completely isolated manner from the main transmission system to increase the reliability of power supply.

As in any power system, stability is a key performance criterion in microgrids. In conventional power systems, mostly SG-based units, operated as so-called grid-forming units, are used for this task. However, in inverter-dominated microgrids, grid-forming capabilities have to be provided by inverter-interfaced sources [5]. Inverters operated in grid-forming mode are commonly represented as ideal controllable AC voltage sources [2], [5]–[7].

While the above is a reasonable assumption, the following important aspect regarding inverter modeling has not been considered explicitly in previous work on microgrid stability analysis, e.g., [8]–[11]. In many practical setups, each individual inverter is operated with its own processor. It is well-known that the clocks used to generate the time signals of the individual processors differ from each other due to clock drifts [12], [13]. Furthermore, it has been argued in [6], [7], [14] that apart from sensor uncertainties, the presence of clock drifts is the main reason why inverters operated with fixed electrical frequency cannot operate in parallel—unless the network possesses a very accurate clock synchronization system, which is rarely the case in practice [7].

The present paper provides an analysis of the effects of clock inaccuracies on microgrid performance in terms of stability and active power sharing. In that regard, our main contributions are: first, we derive a model of an inverter with unknown constant clock drift; second, under a mild assumption on the network topology, we prove the abovementioned claim in [6], [7], [14] that clock inaccuracies hamper synchronization in an inverter-based microgrid, in which the inverters are operated with a fixed uniform constant electrical frequency; third, as indicated in [14], we show that the usual droop controls, see, e.g., [7], [15], render stability of inverter-based microgrids robust with respect to unknown constant clock drifts. The claim is established based on our previous stability analysis of droop-controlled microgrids with ideal clocks [10]. Furthermore, we discuss the effect of clock drifts on active power sharing and illustrate the analysis via a simulation example.

II. Preliminaries

A. Notation

We define the sets $\bar{n} := \{1, 2, \dots, n\}$, $\mathbb{R}_{\geq 0} := \{x \in \mathbb{R} | x \geq 0\}$, $\mathbb{R}_{>0} := \{x \in \mathbb{R} | x > 0\}$, $\mathbb{R}_{\leq 0} := \{x \in \mathbb{R} | x \leq 0\}$, $\mathbb{R}_{<0} := \{x \in \mathbb{R} | x < 0\}$ and $\mathbb{S} := [0, 2\pi)$. For a set $\mathcal{V}$, let $|\mathcal{V}|$ denote its cardinality. For a set of, possibly unordered, positive natural numbers $\mathcal{V} = \{l, k, \dots, n\}$, the short-hand $i \sim \mathcal{V}$ denotes $i = l, k, \dots, n$. Let $x := \text{col}(x_i) \in \mathbb{R}^n$ denote a vector with entries x_i for $i \sim \bar{n}$, $\underline{0}_n$ the zero vector, $\mathbb{1}_n$ the vector with all entries equal to one, I_n the $n \times n$ identity matrix, $0_{n \times n}$ the $n \times n$ matrix with all entries equal to zero and $\text{diag}(a_i), i \sim \bar{n}$, an $n \times n$ diagonal matrix with diagonal entries $a_i \in \mathbb{R}$. Let j denote the imaginary unit. Finally, ∇f denotes the transpose of the gradient of a function $f : \mathbb{R}^n \to \mathbb{R}$.

J. Schiffer is with Technische Universität Berlin, Germany, schiffer@control.tu-berlin.de

R. Ortega is with Laboratoire des Signaux et Systémes, École Supérieure d'Electricité (SUPELEC), Gif-sur-Yvette 91192, France, ortega@lss.supelec.fr

C. A. Hans is with Technische Universität Berlin & Younicos AG, Berlin, Germany, hans@control.tu-berlin.de

J. Raisch is with Technische Universität Berlin & Max-Planck-Institut für Dynamik komplexer technischer Systeme, Germany, raisch@control.tu-berlin.de

B. Electrical network

We consider a Kron-reduced [16] representation of a generic meshed microgrid in which loads are modeled by constant impedances. The Kron-reduced microgrid is formed by $n \geq 1$ nodes, each of which represents a DG unit interfaced via an AC inverter. We denote the set of network nodes by $\bar{n}$ and associate a time-dependent phase angle $\delta_i : \mathbb{R}_{\geq 0} \to \mathbb{S}$ and a voltage amplitude $V_i : \mathbb{R}_{\geq 0} \to \mathbb{R}_{>0}$ to each node $i \in \bar{n}$. We assume that the microgrid is connected, i.e., that for all pairs $(i,k) \in \bar{n} \times \bar{n}$, $i \neq k$, there exists an ordered sequence of nodes from i to k such that any pair of consecutive nodes in the sequence is connected by a power line represented by an admittance. This assumption is reasonable for a microgrid, unless severe line outages separating the system into several disconnected parts occur.

Furthermore, we assume that the admittances in the microgrid are purely inductive. For the line admittances, this assumption is justified if the inductive inverter output impedance (due to the output inductor and/or the possible presence of an output transformer) dominates the resistive parts of the network lines [8], [10]. With regards to the shunt admittances, we are aware that in the case of the Kron-reduced network the reduced network admittance matrix does, in general, not permit to neglect the shunt conductances and our stability results might therefore be inaccurate.

Two nodes i and k of the microgrid are connected via a complex nonzero admittance $Y_{ik} := jB_{ik} \in \mathbb{C}$ with susceptance $B_{ik} \in \mathbb{R}_{<0}$. For convenience, we define $Y_{ik} := 0$ whenever i and k are not directly connected. The set of neighbors of a node $i \in \bar{n}$ is denoted by $\bar{n}_i := \{k \mid k \in \bar{n},\ k \neq i\ , Y_{ik} \neq 0\}$. For ease of notation, we write angle differences as $\delta_{ik} := \delta_i - \delta_k$. The overall active and reactive power flows $P_i : \mathbb{S}^n \times \mathbb{R}^n_{>0} \to \mathbb{R}$ and $Q_i : \mathbb{S}^n \times \mathbb{R}^n_{>0} \to \mathbb{R}$ at a node $i \in \bar{n}$ are obtained as[1]

$$\begin{aligned} P_i &= \sum_{k \sim \bar{n}_i} |B_{ik}| V_i V_k \sin(\delta_{ik}), \\ Q_i &= |B_{ii}| V_i^2 - \sum_{k \sim \bar{n}_i} |B_{ik}| V_i V_k \cos(\delta_{ik}), \end{aligned} \tag{II.1}$$

with

$$B_{ii} := \hat{B}_{ii} + \sum_{k \sim \bar{n}_i} B_{ik}, \tag{II.2}$$

where $\hat{B}_{ii} \in \mathbb{R}_{\leq 0}$ denotes the shunt admittance at the i-th node. As we are mainly concerned with dynamics of DG units, we express all power flows in generator convention.

C. Model of an inverter with ideal clock

Under the assumption of ideal clocks, the grid-forming inverter at the i-th node, $i \in \bar{n}$, can be modeled as an AC voltage source, the frequency and amplitude of which can be specified by the designer[2] [5], [9], i.e.,

$$\begin{aligned} \dot{\delta}_i &= u_i^{\delta}, \\ \tau_{P_i} \dot{P}_i^m &= -P_i^m + P_i, \\ V_i &= u_i^V, \\ \tau_{P_i} \dot{Q}_i^m &= -Q_i^m + Q_i, \end{aligned} \tag{II.3}$$

where $u_i^{\delta} : \mathbb{R}_{\geq 0} \to \mathbb{R}$ and $u_i^V : \mathbb{R}_{\geq 0} \to \mathbb{R}$ are controls. Furthermore, it is assumed that the power outputs P_i and Q_i given in (II.1) are measured and passed through filters with time constant $\tau_{P_i} \in \mathbb{R}_{>0}$ [17]. The measured powers are denoted by $P_i^m : \mathbb{R}_{\geq 0} \to \mathbb{R}$ and $Q_i^m : \mathbb{R}_{\geq 0} \to \mathbb{R}$.

[1] To simplify notation the time argument of all signals is omitted.

[2] An underlying assumption to this model is that whenever the inverter connects an intermittent renewable generation source, e.g., a photovoltaic plant, to the network, it is equipped with some sort of storage (e.g. a battery). Thus, it can increase and decrease its power output within a certain range.

III. Problem statement

In a practical setup, the dynamics (II.3) together with the controllers generating the signals u_i^{δ} and u_i^V are implemented on a processor by means of numerical integration. After each integration step, the generated values of the angle δ_i and the voltage amplitude V_i are passed to the internal controllers of the inverter at the i-th node. These internal controls then ensure that the inverter provides the desired sinusoidal voltage at its terminals [6].

For each unit in the network, the sampling interval used to perform this numerical integration stems from the internal clock of the processor of that same unit. Following standard terminology and to avoid confusions with the electrical frequency, we denote by clock rate the frequency at which the processor is running. The clock rate is usually determined by some sort of resonator, e.g., a crystal oscillator. Almost all resonators suffer from precision inaccuracies [12], [18]. As a consequence, the clocks of different units in the network are not synchronized per se. In particular, this implies that the numerical integration required to implement (II.3) is carried out using different integration time steps at the different units in the network. The impact of this phenomenon on microgrid performance in terms of stability and active power sharing is analyzed in the following.

IV. Model of an inverter with inaccurate clock

In this section, an equivalent model to (II.3) is derived for an inverter with an inaccurate processor clock. For an illustration of the influence of the clock inaccuracy on the numerical integration of (II.3), consider the well-known Euler method [19] as an exemplary numerical integration method[3]. Let $x \in \mathbb{R}^n$, $f : \mathbb{R} \times \mathbb{R}^n \to \mathbb{R}^n$ and consider the ordinary differential equation

$$\dot{x}(t) = f(t, x(t)), \quad x(t_0) = x_0.$$

Fix an initial time $t_0 \in \mathbb{R}$ and an integration step size $h \in \mathbb{R}_{>0}$. Let $k \in \mathbb{N}$ be the k-th integration step. Then

$$t^k = t_0 + kh \tag{IV.1}$$

and the integration step of the Euler method from t^k to $t^{k+1} = t^k + h$ is given by [19]

$$x^{k+1} = x^k + hf(t^k, x^k). \tag{IV.2}$$

Recall that at each inverter the integration (IV.2) is carried out using the time signal provided by the local clock. As outlined in Section III, almost all real clocks exhibit a certain (though often small) inaccuracy. In data-sheets, this clock drift is usually specified relative to the nominal clock rate [18]. To see how such a clock drift affects the time signal provided by a processor clock, denote an exemplary nominal clock rate by $f_c \in \mathbb{R}_{>0}$ and its relative drift by $\mu \in \mathbb{R}$. Typically, $|\mu| \leq 10^{-5}$ [18]. Then, the actual sampling interval $\Delta t_c \in \mathbb{R}_{>0}$

[3] Our analysis and model derivation apply equivalently to other numerical integration methods, at the cost of a more complex notation.

with respect to the nominal sampling interval $\Delta\bar{t}_c = 1/f_c$ of the corresponding processor is

$$\Delta t_c = \frac{1}{f_c(1+\mu)} = \frac{1}{1+\mu}\Delta\bar{t}_c = (1+\epsilon)\Delta\bar{t}_c, \qquad \text{(IV.3)}$$

with $\epsilon := -\mu/(1+\mu)$. Note that both the step size h in (IV.1) and the time signal provided by the processor (given, e.g., by (IV.1)) are multiples of the sampling time Δt_c in (IV.3). Denote by $t \in \mathbb{R}$ the nominal network time, by $t_0 \in \mathbb{R}$ the nominal network initial time, by $h \in \mathbb{R}_{>0}$ the step size in nominal time, by $t_i \in \mathbb{R}$ the local time of the clock of the i-th inverter, by $t_{i_0} \in \mathbb{R}$ its initial time and by $h_i \in \mathbb{R}_{>0}$ its step size. Furthermore, denote the relative drift of the clock of the i-th inverter by $\mu_i \in \mathbb{R}$. Due to the good short-term accuracy of many resonators (see Section III), we assume in the following that μ_i is a small, but unknown constant parameter satisfying $|\mu_i| \ll 1$. Furthermore, we account for a possible constant local clock offset $\bar{\zeta}_i \in \mathbb{R}$. Without loss of generality, it is convenient to write $\bar{\zeta}_i$ as $\bar{\zeta}_i = t_0\epsilon_i + \zeta_i$, $\zeta_i \in \mathbb{R}$. Hence, with (IV.3), t_{i_0} and h_i can be expressed as

$$t_{i_0} = t_0 + \bar{\zeta}_i = t_0(1+\epsilon_i) + \zeta_i, \quad h_i = h(1+\epsilon_i).$$

Then

$$t_i^k = t_{i_0} + kh_i = t^k(1+\epsilon_i) + \zeta_i,$$

with t^k given in (IV.1). It follows that, for sufficiently fast sampling times, the clock drift of the processor of the i-th inverter can formally be included in the continuous-time model (II.3) by an appropriate time-scaling, i.e.,

$$t_i = (1+\epsilon_i)t + \zeta_i. \qquad \text{(IV.4)}$$

Note that the clock model (IV.4) is identical to that used to investigate clock synchronization, e.g., in [13]. Furthermore,

$$\frac{d(\cdot)}{dt_i} = \frac{1}{(1+\epsilon_i)}\frac{d(\cdot)}{dt} = \gamma_i\frac{d(\cdot)}{dt},\ \gamma_i := \frac{1}{1+\epsilon_i} = 1+\mu_i > 0. \qquad \text{(IV.5)}$$

Suppose the time derivatives in (II.3) are expressed with respect to the local time t_i of the i-th inverter. Inserting (IV.5) in (II.3) yields

$$\begin{aligned} \gamma_i\dot{\delta}_i &= u_i^\delta, \\ \gamma_i\tau_{P_i}\dot{P}_i^m &= -P_i^m + P_i, \\ V_i &= u_i^V, \\ \gamma_i\tau_{P_i}\dot{Q}_i^m &= -Q_i^m + Q_i, \end{aligned} \qquad \text{(IV.6)}$$

where the time derivatives are now expressed with respect to the nominal time t. Furthermore, without loss of generality, the local clock offset ζ_i can be included in the initial conditions of the system (IV.6) and is therefore omitted in the following analysis. By defining (with P_i, Q_i in (II.1))

$$\begin{aligned} &\delta := \mathrm{col}(\delta_i) \in \mathbb{S}^n, && V := \mathrm{col}(V_i) \in \mathbb{R}^n_{>0}, \\ &u^\delta := \mathrm{col}(u_i^\delta) \in \mathbb{R}^n, && u^V := \mathrm{col}(u_i^V) \in \mathbb{R}^n, \\ &P := \mathrm{col}(P_i) \in \mathbb{R}^n, && Q := \mathrm{col}(Q_i) \in \mathbb{R}^n, \\ &\Gamma := \mathrm{diag}(\gamma_i) \in \mathbb{R}^{n\times n}, && T := \mathrm{diag}(\tau_{P_i}) \in \mathbb{R}^{n\times n}, \end{aligned}$$

the system (IV.6) can be compactly written as

$$\begin{aligned} \Gamma\dot{\delta} &= u^\delta, \\ \Gamma T\dot{P}^m &= -P^m + P, \\ V &= u^V, \\ \Gamma T\dot{Q}^m &= -Q^m + Q. \end{aligned} \qquad \text{(IV.7)}$$

The result below proves, under a mild assumption on the network topology, that a microgrid operated with constant frequencies does not possess a solution with constant power flows in the presence of clock inaccuracies described above.

Claim 4.1: Consider the system (IV.7), (II.1). Assume $\gamma_i \neq \gamma_k$, $i \sim \bar{n}$, $k \sim \bar{n}_i$ and that there is at least one node $i \in \bar{n}$ with $|\bar{n}_i| \leq 2$. Set $u_i^\delta = \omega^d$ and $u_i^V = V^d$, $i \sim \bar{n}$, where ω^d and V^d are positive real constants. Then the system (IV.7), (II.1) possesses no solution

$$\mathrm{col}(\delta^*, P^{m,*}, V^d, Q^{m,*}),$$

where $P^{m,*} \in \mathbb{R}^n$ and $Q^{m,*} \in \mathbb{R}^n$ are constant vectors.

Proof: Recall that the power flow equations (II.1) depend upon angle differences δ_{ik}^*. From (IV.7) with $u_i^\delta = \omega^d$, $i \sim \bar{n}$, it follows that

$$\delta_{ik}^* = \delta_{ik}^*(0) + \omega^d t\left(\frac{1}{\gamma_i} - \frac{1}{\gamma_k}\right), \quad i \sim \bar{n},\, k \sim \bar{n}_i. \qquad \text{(IV.8)}$$

Hence, with the made assumptions, $\dot{\delta}_{ik}^*$ is a nonzero constant and clearly the absolute angle differences grow with time.

We proceed by showing by contradiction that (IV.8) implies non-existence of solutions of (IV.7), (II.1) with constant vectors $P^{m,*} \in \mathbb{R}^n$ and $Q^{m,*} \in \mathbb{R}^n$. Assume that such a solution exists and let $P_i^{m,*}$ be the constant active power measurement corresponding to the i-th node with $|\bar{n}_i| = 2$. Then, we have from (IV.7) with $u_i^V = V^d$, $i \sim \bar{n}$,

$$|B_{ik}|(V^d)^2\sin(\delta_{ik}^*) + |B_{im}|(V^d)^2\sin(\delta_{im}^*) = P_i^{m,*}. \qquad \text{(IV.9)}$$

Taking the time derivative of (IV.9) yields

$$|B_{ik}|(V^d)^2\dot{\delta}_{ik}^*\cos(\delta_{ik}^*) + |B_{im}|(V^d)^2\dot{\delta}_{im}^*\cos(\delta_{im}^*) = 0, \qquad \text{(IV.10)}$$

where $\dot{\delta}_{ik}^*$ and $\dot{\delta}_{im}^*$ are nonzero constants. This implies that

$$\cos(\delta_{ik}^*) = 0 \ \Leftrightarrow\ \cos(\delta_{im}^*) = 0.$$

Hence, $\dot{\delta}_{ik}^* = \dot{\delta}_{im}^*$. But, since $\gamma_i \neq \gamma_k \neq \gamma_m$, $\dot{\delta}_{ik}^* \neq \dot{\delta}_{im}^*$. Thus, (IV.10) is violated.

A similar argument applies to the reactive power flows Q given in (II.1). Furthermore, for $|\bar{n}_i| = 1$ the result follows trivially from (IV.9). Consequently, the system (IV.7), (II.1) possesses no synchronized motion with constant vectors $P^{m,*}$ and $Q^{m,*}$, completing the proof. ∎

Claim 4.1 confirms the observation made in [6], [7], [14] that, if several inverters in parallel are to be operated with a constant uniform frequency, then a very accurate clock synchronization system is required in order to maintain constant angle differences. See [7] for a discussion on possible solutions for this.

Remark 4.2: The requirement $u_i^V = V^d$, $i \sim \bar{n}$, is merely added in Claim 4.1 to simplify the presentation of the proof.

V. Droop control renders inverter-based microgrids robust to clock drifts

In addition to the sensitivity with respect to clock drifts, operating parallel grid-forming inverters with fixed constant frequencies (and voltage amplitudes) has two further main disadvantages. First, the network operator looses all controllability over the current and power flows in the network (unless the phase angles are directly controlled, which again requires a very accurate synchronization system [7]). Hence, the control objective of power sharing can, in general, not be achieved. Second, such an operation may lead to very high uncontrolled current flows in the network.

A popular control scheme to address both aforementioned problems is droop control [7], [15]. While there exists a large variety of control schemes for inverters named droop control, the ones most commonly employed are defined as follows [7]. Let $\omega^d \in \mathbb{R}_{>0}$, $V^d \in \mathbb{R}^n_{>0}$ and

$$K_P = \text{diag}(k_{P_i}) \in \mathbb{R}^{n\times n}_{>0},\ K_Q = \text{diag}(k_{Q_i}) \in \mathbb{R}^{n\times n}_{>0},$$
$$P^d = \text{col}(P^d_i) \in \mathbb{R}^n,\ Q^d = \text{col}(Q^d_i) \in \mathbb{R}^n.$$

Then, the usual frequency and voltage droop controls are

$$\begin{aligned} u^\delta &= \omega^d \mathbb{1}_n - K_P(P^m - P^d), \\ u^V &= V^d - K_Q(Q^m - Q^d). \end{aligned} \tag{V.1}$$

We refer the reader to [8], [9] for an in-depth discussion and motivation of the control (V.1). By inserting (V.1) in (IV.6) and following [9], [10], we obtain the closed-loop system

$$\begin{aligned} \Gamma\dot\delta &= \omega, \\ \Gamma T\dot\omega &= -\omega + \omega^d\mathbb{1}_n - K_P(P - P^d), \\ \Gamma T\dot V &= -V + V^d - K_Q(Q - Q^d), \end{aligned} \tag{V.2}$$

where P and Q are given in (II.1) and $\omega := \text{col}(\omega_i) \in \mathbb{R}^n$ is the vector of internal inverter frequencies. Note that the model (V.2), (II.1) differs from the model of a droop-controlled inverter-based microgrid with ideal clocks analyzed in [8]–[11] by the coefficients γ_i, $i \sim \bar n$.

A. Synchronized motion under clock drifts

It is convenient to introduce the notion of a desired synchronized motion of the system (V.2), (II.1).

Definition 5.1: A solution $\text{col}(\delta^s, \omega^s, V^s) \in \mathbb{S}^n \times \mathbb{R}^n \times \mathbb{R}^n_{>0}$ of the system (V.2), (II.1) is said to be a desired synchronized motion if $\omega^s \in \mathbb{R}^n$ and $V^s \in \mathbb{R}^n_{>0}$ are constant vectors and $\delta^s \in \Theta$, where

$$\Theta := \left\{ \delta \in \mathbb{S}^n \;\middle|\; |\delta_{ik}| < \frac{\pi}{2}, i \sim \bar n,\ k \sim \bar n_i \right\},$$

such that $\delta^s_{ik} = \delta^s_i - \delta^s_k$ are constant, $i \sim \bar n$, $k \sim \bar n_i, \forall t \geq 0$.

Claim 5.2: Consider the system (V.2), (II.1). The vector of internal frequencies ω^s of any desired synchronized motion is given uniquely by

$$\omega^s = \Gamma\omega^N\mathbb{1}_n, \tag{V.3}$$

where the real constant ω^N is given by

$$\omega^N = \omega^d \frac{\sum_{i\sim\bar n} \frac{1}{k_{P_i}}}{\sum_{i\sim\bar n} \frac{\gamma_i}{k_{P_i}}} + \frac{\sum_{i\sim\bar n} P^d_i}{\sum_{i\sim\bar n} \frac{\gamma_i}{k_{P_i}}}. \tag{V.4}$$

Proof: By Definition 5.1, a synchronized motion of the system (V.2), (II.1) is characterized by constant vectors ω^s and V^s, as well as constant angle differences δ^s_{ik}. Since,

$$\delta^s_{ik} = \delta^s_{ik}(0) + \left(\frac{\omega^s_i}{\gamma_i} - \frac{\omega^s_k}{\gamma_k}\right) t, \quad i \sim \bar n, \quad k \sim \bar n_i,$$

constant angle differences, together with the connectedness of the network, imply

$$\frac{\omega^s_i}{\gamma_i} = \frac{\omega^s_k}{\gamma_k} =: \omega^N, \quad i \sim \bar n, \quad k \sim \bar n. \tag{V.5}$$

Moreover, it follows from (V.2), (II.1) with $\dot\omega^s = \underline 0_n$ that

$$0 = \mathbb{1}_n^T \left(K_P^{-1}(-\omega^s + \omega^d\mathbb{1}_n) + P^d\right),$$

which with (V.5) is equivalent to

$$0 = \sum_{i\sim\bar n} \left(\frac{1}{k_{P_i}}(-\gamma_i\omega^N + \omega^d) + P^d_i\right)$$

and, by rearranging terms, yields (V.4). ∎

Note that for $\gamma_i = 1$, $i \sim \bar n$, i.e., for ideal clocks, all internal frequencies become identical and (V.4) reduces to the usual expression of the synchronization frequency in a lossless microgrid, see [8], [10]. Hence, under the presence of clock drifts, the internal synchronized frequencies of the inverters are scaled by the parameters $1/\gamma_i$, $i \sim \bar n$.

B. Error states

The stability analysis is carried out following [10]. To establish the result, we make the following natural power-balance feasibility assumption.

Assumption 5.3: The system (V.2), (II.1) possesses a desired synchronized motion.

Under Assumption 5.3, we introduce the error states

$$\tilde\omega(t) := \omega(t) - \omega^s, \quad \tilde\delta(t) := \delta(0) + \Gamma^{-1}\int_0^t \tilde\omega(\tau)d\tau.$$

Furthermore, by noting that the power flows (II.1) only depend upon angle differences, we express all angles relative to an arbitrarily chosen reference node, say node n, i.e.,

$$\theta := \mathcal{R}\tilde\delta, \quad \mathcal{R} := \begin{bmatrix} I_{(n-1)} & -\mathbb{1}_{(n-1)} \end{bmatrix}.$$

For ease of notation, we define the constant $\theta_n := 0$, which is not part of the vector θ. The power flows (II.1) become in the reduced coordinates $x := \text{col}(\theta, \tilde\omega, V) \in \mathbb{R}^{n-1} \times \mathbb{R}^n \times \mathbb{R}^n_{>0}$

$$\begin{aligned} \mathcal{P}_i &:= \sum_{k\sim\bar n_i} V_iV_k|B_{ik}|\sin(\theta_{ik}), \\ \mathcal{Q}_i &:= |B_{ii}|V_i^2 - \sum_{k\sim\bar n_i} V_iV_k|B_{ik}|\cos(\theta_{ik}), \quad i \sim \bar n, \\ \mathcal{P} &:= \text{col}(\mathcal{P}_i) \in \mathbb{R}^n, \quad \mathcal{Q} := \text{col}(\mathcal{Q}_i) \in \mathbb{R}^n. \end{aligned} \tag{V.6}$$

To simplify notation, we also introduce the constants

$$c_{1_i} := \omega^d - \omega^s_i + k_{P_i}P^d_i,\ c_{2_i} := V^d_i + k_{Q_i}Q^d_i,\ i \sim \bar n$$

and $c_1 := \text{col}(c_{1_i}) \in \mathbb{R}^n$ and $c_2 := \text{col}(c_{2_i}) \in \mathbb{R}^n$. In the reduced coordinates, the dynamics (V.2), (V.6) are given by

$$\begin{aligned} \dot\theta &= \mathcal{R}\Gamma^{-1}\tilde\omega, \\ \Gamma T\dot{\tilde\omega} &= -\tilde\omega - K_P\mathcal{P} + c_1, \\ \Gamma T\dot V &= -V - K_Q\mathcal{Q} + c_2, \end{aligned} \tag{V.7}$$

The reduced system (V.7), (V.6) has an equilibrium at $x^s := \text{col}(\theta^s, \underline 0_n, V^s)$, the asympotitic stability of which implies asymptotic convergence to the synchronized motion (up to a uniform shift of all angles). Note that from (V.7), (V.6) it follows that, along any synchronized motion,

$$\mathbb{1}_n^T\mathcal{P} = \mathbb{1}_n^TK_P^{-1}c_1 = 0 \;\Rightarrow\; c_{1n} = -\sum_{i=1}^{n-1}\frac{k_{P_n}}{k_{P_i}}c_{1_i}. \tag{V.8}$$

C. Main result

For the presentation of our main result, it is convenient to introduce the matrices $\mathcal{L} \in \mathbb{R}^{(n-1)\times(n-1)}$, $\mathcal{W} \in \mathbb{R}^{(n-1)\times n}$, $\mathcal{D} \in \mathbb{R}^{n\times n}$ and $\mathcal{T}(\delta^s) \in \mathbb{R}^{n\times n}$ defined in the appendix.

Proposition 5.4: Consider the system (V.7), (II.1) with Assumption 5.3. Fix τ_{P_i}, k_{P_i} and P^d_i, $i \sim \bar n$. If V^d_i, k_{Q_i} and Q^d_i are selected such that

$$\mathcal{D} + \mathcal{T}(\delta^s) - \mathcal{W}^\top\mathcal{L}^{-1}\mathcal{W} > 0, \tag{V.9}$$

then the equilibrium point x^s is locally asymptotically stable.

Proof: As done in [10], the claim is established by following the interconnection and damping assignment passivity-based control approach [20]. With $x = \text{col}(\theta, \tilde\omega, V)$

and by recalling (V.8), the system (V.7), (V.6) can be written in port-Hamiltonian form, i.e.,

$$\dot{x} = (J - R(x))\nabla H$$

with Hamiltonian $H : \mathbb{R}^{(n-1)} \times \mathbb{R}^n \times \mathbb{R}^n_{>0} \to \mathbb{R}$ given by

$$H(x) = \sum_{i=1}^{n} \Big(\frac{\tau_{P_i}}{2k_{P_i}} \tilde{\omega}_i^2 + \frac{1}{k_{Q_i}} (V_i - c_{2_i} \ln(V_i)) + \frac{1}{2} |B_{ii}| V_i^2 - \frac{1}{2} \sum_{k \sim \bar{n}_i} V_i V_k |B_{ik}| \cos(\theta_{ik}) \Big) - \sum_{i=1}^{n-1} \frac{c_{1_i}}{k_{P_i}} \theta_i, \quad \text{(V.10)}$$

interconnection matrix

$$J = \begin{bmatrix} 0_{(n-1)\times(n-1)} & \mathcal{J} \\ -\mathcal{J}^\top & 0_{2n\times 2n} \end{bmatrix},$$

$$\mathcal{J} = \begin{bmatrix} \mathcal{R} K_P (\Gamma T)^{-1} & 0_{(n-1)\times n} \end{bmatrix},$$

and damping matrix

$$R = \text{diag}(\underline{0}_{(n-1)}, K_P(\Gamma T^2)^{-1} \mathbb{1}_n, K_Q (\Gamma T)^{-1} V).$$

Note that the Hamiltonian $H(x)$ defined in (V.10) is identical to that for droop-controlled microgrids with ideal clocks derived in the proof of Proposition 5.9 in [10]. The parameters γ_i, $i \sim \bar{n}$, stemming from the clock drifts only appear as scaling parameters in the interconnection and damping matrices J and R. Furthermore, it has been proven in [10] that, under the standing assumptions, $\mathcal{L}$ is positive definite. It also follows from (II.2) that $\mathcal{T}(\delta^s)$ is positive semidefinite. Consequently, local asympotitic stability of the equilibrium point x^s of the system (V.7), (V.6) follows in a straightforward manner from the proof of Proposition 5.9 in [10]. ∎

Condition (V.9) is independent of the parameters γ_i, $i \sim \bar{n}$, originating from the clock drifts. This fact implies that local stability of the equilibrium x^s is independent from γ_i, i.e., stability of an inverter-based droop-controlled microgrid is robust with respect to unknown constant clock drifts.

VI. Clock drifts and active power sharing

We employ the following definition of power sharing.

Definition 6.1: Let $\chi_i \in \mathbb{R}_{>0}$ denote weighting factors and P_i^s the steady-state active power flow, $i \sim \bar{n}$. Then, two inverters at nodes i and k are said to share their active powers proportionally according to χ_i and χ_k, if

$$\frac{P_i^s}{\chi_i} = \frac{P_k^s}{\chi_k}.$$

For droop-controlled inverters with ideal clocks, it has been shown in [8], [10] that the objective of active power sharing is achieved in a synchronized state if the parameters of the frequency droop controllers are chosen such that

$$k_{P_i}\chi_i = k_{P_k}\chi_k \text{ and } k_{P_i} P_i^d = k_{P_k} P_k^d. \quad \text{(VI.1)}$$

The result below quantizes the largest ratio of weighted power outputs P_i^s/χ_i introduced by the clock drifts μ_i if the parameters k_{P_i} and P_i^d are chosen according to (VI.1). Due to space limitations, we restrict the statement to units with positive active power outputs.

Claim 6.2: Consider the system (V.2), (II.1). Assume that it possesses a synchronized motion with vector of synchronization frequencies $\omega^s \in \mathbb{R}^n_{>0}$. Let $\hat{n} \subseteq \bar{n}$. Fix χ_i and select the parameters k_{P_i} and P_i^d according to (VI.1), $i \sim \hat{n}$. Then the largest ratio of weighted power outputs P_i^s/χ_i, $i \sim \hat{n}$, satisfying $\text{sign}(P_i^s) = \text{sign}(P_k^s) = 1$, is given by

$$\frac{\max_{i\sim\hat{n}} (P_i^s/\chi_i)}{\min_{k\sim\hat{n}} (P_k^s/\chi_k)} = \frac{-\min_{i\sim\hat{n}}(\mu_i)\omega^N + c}{-\max_{k\sim\hat{n}}(\mu_k)\omega^N + c} \quad \text{(VI.2)}$$

with $c = k_{P_i} P_i^d + \omega^d - \omega^N$, $i \sim \hat{n}$ and ω^N defined in (V.4).

Proof: Recall from (IV.5) that $\gamma_i = 1 + \mu_i$. This implies with (V.3) and (V.4) that $\omega_i^s = \gamma_i \omega^N = (1 + \mu_i)\omega^N$. Hence, for any pair of nodes $(i, k) \in \hat{n} \times \hat{n}$, $i \neq k$, satisfying (VI.1), the ratio of their weighted active power outputs along the synchronized motion of the system (V.2), (II.1) is given by

$$\frac{P_i^s/\chi_i}{P_k^s/\chi_k} = \frac{(-\omega_i^s + k_{P_i} P_i^d + \omega^d) k_{P_k}\chi_k}{(-\omega_k^s + k_{P_k} P_k^d + \omega^d) k_{P_i}\chi_i} = \frac{-\mu_i\omega^N + c}{-\mu_k\omega^N + c}. \quad \text{(VI.3)}$$

Finally, with $\omega^N \in \mathbb{R}^n_{>0}$, (VI.2) follows from (VI.3). ∎

Condition (VI.2) reveals that the presence of unknown clock drifts has a deteriorating effect on the active power sharing accuracy. Nevertheless, since in general $|\mu_i| \ll 1$, (VI.2) also shows that the introduced error in power sharing is negligible in most practical scenarios. Therefore, the selection criteria (VI.1) seem also appropriate in the presence of clock drifts.

VII. Simulation example

The conducted analysis is illustrated via a simulation example based on the three-phase islanded Subnetwork 1 CIGRE MV benchmark model [21]. The network, shown in Fig. 1, is composed of 11 main buses and possesses a total of 6 generation units operated in grid-forming mode. The power ratings of these units are given by $S_i^N = [0.505, 0.028, 0.261, 0.179, 0.168, 0.012]$ pu, where pu denotes per unit values with respect to the system base power $S_{\text{base}} = 4.75$ MVA. For a detailed description of the simulation setup, the reader is referred to [21] and [10].

Besides illustrating the effect of clock drifts in inverter-based microgrids, the simulation also serves to evaluate the robustness of the model (II.1), (V.2) and the stability condition (V.9) with respect to model uncertainties. Therefore, loads are represented by impedances and all inductances are modeled by first-order ODEs opposed to constant admittances as in (II.1). The simulation is carried out in Plecs.

The relative clock drifts are assumed as $\mu = [1, -10^{-3}, -10^{-1}, 1, 10^{-2}, -10^{-1}]10^{-5}$. At first, the inverters are operated with a fixed constant frequency $\omega^d = 2\pi 50$ Hz and fixed voltage amplitudes $V^d = 1$ pu. In this scenario, the power outputs of the inverters oscillate, see Fig. 2. This illustrates that clock drifts hamper synchronization, when all inverters are operated with a uniform constant electrical frequency. Note that we have not considered power limitations. In a real microgrid, any source exceeding its nominal power output would have been disconnected by the overcurrent protection devices.

For the case of a droop-controlled microgrid, following (VI.1), we set $\chi_i = S_i^N$, $P_i^d = 0.6 S_i^N$ pu and $k_{P_i} = 0.2/S_i^N$ Hz/pu, $i \sim \bar{n}$. The parameters of the voltage droop controllers are chosen as $Q_i^d = 0.25 S_i^N$ pu, $k_{Q_i} = 0.1/S_i^N$ pu/pu and $V_i^d = 1$ pu, $i \sim \bar{n}$. The simulation example in Fig. 3 shows that under the droop controls (V.1), the microgrid converges quickly to a synchronized motion—despite the presence of clock drifts. As in our previous investigation [10], the stability condition (V.9) is satisfied, indicating that it is, to a certain extent, robust to model uncertainties, such as conductances. The largest ratio of

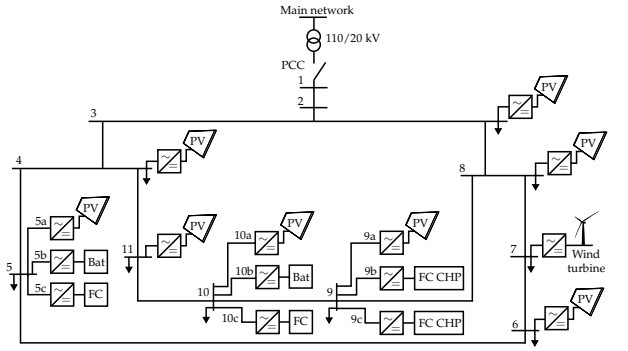

Fig. 1. Benchmark model adapted from [21] with 11 main buses and inverter–interfaced units of type: PV–Photovoltaic, FC–fuel cell, Bat–battery, FC CHP. PCC denotes the point of common coupling to the main grid. The sign ↓ denotes loads.

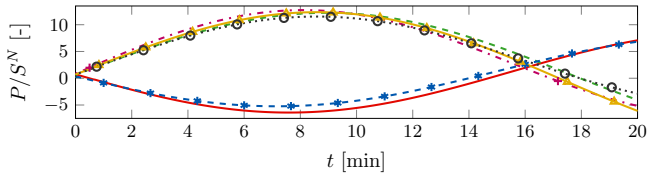

Fig. 2. Simulation example of a microgrid in which the inverters exhibit clock drifts and are operated with constant uniform frequency $\omega^d = 2\pi 50$ Hz and constant voltage amplitude of $V^d = 1$ pu.

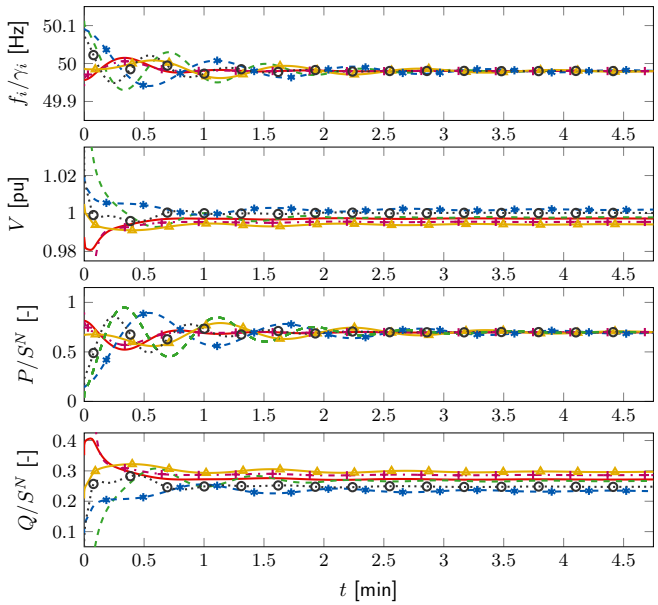

Fig. 3. Simulation example of a droop-controlled microgrid with clock drifts. Trajectories of the power outputs relative to source rating P_i/S_i^N and Q_i/S_i^N, the internal scaled frequencies $f_i = 2\pi\omega_i/\gamma_i$ in Hz and the voltage amplitudes V_i in pu of the controllable sources in the microgrid. The lines correspond to the following sources: battery 5b, $i = 1$ '–', FC 5c, $i = 2$ '- -', FC CHP 9b, $i = 3$ '+-', FC CHP 9c, $i = 4$ '* -', battery 10b, $i = 5$ '△ -' and FC 10c, $i = 6$ 'o-'.

weighted active power outputs (VI.2) introduced by the clock drifts μ_i amounts to 1.0085. Hence, the error in active power sharing is negligibly small.

VIII. Conclusion

We have shown that clock drifts are a practically relevant phenomenon in inverter-based microgrids, as they prevent synchronization if the individual grid-forming inverters are operated with a fixed constant electrical frequency. A suitable inverter model incorporating this phenomenon has been provided. By using this model, we have derived a port-Hamiltonian representation of a lossless droop-controlled inverter-based microgrid, based on which we have shown that stability of such networks is robust to unknown constant clock drifts. In future work, we plan to complement the conducted analysis with tests on an experimental setup.

Appendix

The matrix $\mathcal{D}$ is given by

$$\mathcal{D} := \operatorname{diag}\left(\frac{c_{2_m}}{k_{Q_m}(V_m^s)^2}\right) = \operatorname{diag}\left(\frac{V_m^d + k_{Q_m}Q_m^d}{k_{Q_m}(V_m^s)^2}\right), m \sim \bar{n}.$$

The entries of the matrices $\mathcal{L}$, $\mathcal{W}$ and $\mathcal{T}(\delta^s)$ are given by

$$l_{ii} := \sum_{q=1}^{n} |B_{iq}|V_i^s V_q^s \cos(\delta_{iq}^s),\ l_{ik} := -|B_{ik}|V_i^s V_k^s \cos(\delta_{ik}^s),$$

$$w_{ii} := \sum_{q=1}^{n} |B_{iq}|V_q^s \sin(\delta_{iq}^s),\ w_{iq} := |B_{iq}|V_i^s \sin(\delta_{iq}^s),$$

$$t_{pp} := |B_{pp}|, \quad t_{pq} := -|B_{pq}|\cos(\delta_{pq}^s),$$

where $i \sim \bar{n}\setminus\{n\}$, $k \sim \bar{n}\setminus\{n\}$, as well as $p \sim \bar{n}$ and $q \sim \bar{n}$.

References

[1] H. Farhangi, "The path of the smart grid," *IEEE Power and Energy Magazine*, vol. 8, no. 1, pp. 18 –28, january-february 2010.

[2] T. Green and M. Prodanovic, "Control of inverter-based micro-grids," *Elec. Power Sys. Res.*, vol. Vol. 77, no. 9, pp. 1204–1213, july 2007.

[3] R. Lasseter, "Microgrids," in *IEEE PESWM*, 2002, pp. 305 – 308.

[4] N. Hatziargyriou, H. Asano, R. Iravani, and C. Marnay, "Microgrids," *IEEE Power and Energy Magazine*, vol. 5, no. 4, pp. 78–94, 2007.

[5] J. Lopes, C. Moreira, and A. Madureira, "Defining control strategies for microgrids islanded operation," *IEEE Transactions on Power Systems*, vol. 21, no. 2, pp. 916 – 924, may 2006.

[6] J. Rocabert, A. Luna, F. Blaabjerg, and P. Rodriguez, "Control of power converters in AC microgrids," *IEEE Transactions on Power Electronics*, vol. 27, no. 11, pp. 4734–4749, Nov 2012.

[7] J. Guerrero, P. Loh, M. Chandorkar, and T. Lee, "Advanced control architectures for intelligent microgrids - Part I: Decentralized and hierarchical control," *IEEE Transactions on Industrial Electronics*, vol. 60, no. 4, pp. 1254–1262, 2013.

[8] J. W. Simpson-Porco, F. Dörfler, and F. Bullo, "Synchronization and power sharing for droop-controlled inverters in islanded microgrids," *Automatica*, vol. 49, no. 9, pp. 2603 – 2611, 2013.

[9] J. Schiffer, D. Goldin, J. Raisch, and T. Sezi, "Synchronization of droop-controlled microgrids with distributed rotational and electronic generation," in *52nd CDC*, Florence, Italy, 2013, pp. 2334–2339.

[10] J. Schiffer, R. Ortega, A. Astolfi, J. Raisch, and T. Sezi, "Conditions for stability of droop-controlled inverter-based microgrids," *Automatica*, vol. 50, no. 10, pp. 2457–2469, 2014.

[11] U. Münz and M. Metzger, "Voltage and angle stability reserve of power systems with renewable generation," in *19th IFAC World Congress*, 2014, pp. 9075–9080.

[12] H. Kopetz, *Real-time systems: design principles for distributed embedded applications*. Springer, 2011.

[13] L. Schenato and F. Fiorentin, "Average timesynch: A consensus-based protocol for clock synchronization in wireless sensor networks," *Automatica*, vol. 47, no. 9, pp. 1878–1886, 2011.

[14] A. Engler, "Applicability of droops in low voltage grids," *International Journal of Distributed Energy Resources*, vol. 1, no. 1, pp. 1–6, 2005.

[15] M. Chandorkar, D. Divan, and R. Adapa, "Control of parallel connected inverters in standalone AC supply systems," *IEEE Transactions on Industry Applications*, vol. 29, no. 1, pp. 136 –143, jan/feb 1993.

[16] P. Kundur, *Power system stability and control*. McGraw-Hill, 1994.

[17] N. Pogaku, M. Prodanovic, and T. Green, "Modeling, analysis and testing of autonomous operation of an inverter-based microgrid," *IEEE Trans. on Power Electronics*, vol. 22, no. 2, pp. 613 –625, march 2007.

[18] Anritsu, "Understanding frequency accuracy in crystal controlled instruments - application note," Anritsu EMEA Ltd., Tech. Rep., 2001.

[19] J. C. Butcher, *Numerical methods for ordinary differential equations*. John Wiley & Sons, 2008.

[20] R. Ortega, A. v. d. Schaft, B. Maschke, and G. Escobar, "Interconnection and damping assignment passivity-based control of port-controlled Hamiltonian systems," *Automatica*, vol. 38, no. 4, pp. 585–596, 2002.

[21] K. Rudion, A. Orths, Z. Styczynski, and K. Strunz, "Design of benchmark of medium voltage distribution network for investigation of DG integration," in *IEEE PESGM*, 2006.